

## THE FORMATION OF MOLECULES IN PROTOSTELLAR WINDS

A. E. GLASSGOLD, G. A. MAMON,<sup>1</sup> AND P. J. HUGGINS

Department of Physics, New York University, 2 Washington Place, New York, NY 10003

Received 1990 September 7; accepted 1990 October 31

### ABSTRACT

The production and destruction processes for molecules in very fast protostellar winds are analyzed and modeled with a one-dimensional chemical kinetics code. Radial density and temperature distributions suggested by protostellar theory are explored as are a range of mass-loss rates. The efficiency of in situ formation of heavy molecules is found to be high if the wind temperature falls sufficiently rapidly, as indicated by theory. The degree of molecular conversion is a strong function of the mass-loss rate and of density gradients associated with the acceleration and collimation of the wind. Even in cases where essentially all of the heavy atoms are processed into molecules, a significant fraction of atomic hydrogen remains so that highly molecular, protostellar winds are able to emit the 21 cm line. Although CO has a substantial abundance in most models relevant to very young protostars, high abundances of other molecules such as SiO and H<sub>2</sub>O signify more complete association characteristic of winds containing regions of very high density. Although the models apply only to regions close to the protostar, they are in qualitative accord with recent observations at much larger distances of both atomic and molecular emission from extremely high-velocity flow.

*Subject headings:* molecular processes — stars: pre-main-sequence — stars: winds

### 1. INTRODUCTION

Both observations and theory support the idea that very high-velocity winds are generated by newly formed protostars. The most direct evidence is the detection of both atomic hydrogen and carbon monoxide at speeds of up to a few hundred km s<sup>-1</sup> in several low-luminosity protostars (Lizano et al. 1988; Koo 1989). Theoretical notions on the formation of a protostar from an accretion disk also lead to high-velocity winds, generated, for example, by centrifugally driven magnetic stresses (e.g., Shu, Adams, & Lizano 1987). These winds originate close to the protostar and carry fundamental information about the star-formation process out to large distances, where their effects are observed in a variety of phenomena, e.g., in low-velocity, bipolar, molecular outflows (Lada 1985; Snell 1987). Observations also suggest that low-luminosity protostars produce partially recombined winds (Natta et al. 1988). We are thus led to investigate in this paper both the ionization and the molecular properties of the primary winds generated by protostars.

In an earlier paper (Glassgold, Mamon, & Huggins 1989, henceforth Paper I), we concluded that molecular synthesis in protostellar winds can be efficient, in contrast to the work of Rawlings, Williams, & Canto (1988). Our preliminary results were based on ad hoc representations of the wind properties, dictated by the absence of temperature information. Paper I prompted Ruden, Glassgold, & Shu (1990, henceforth RGS) to investigate the heating and cooling of the protostellar winds of very young, low-luminosity protostars, for which the theory is sufficiently developed that the dynamics can be reasonably well-specified (see, e.g., Shu et al. 1987). According to this theory, the protostar and the accretion disk corotate at the protostellar breakup speed so that there is no accretion shock (a condition that is not likely to be satisfied during later stages of protostellar evolution). RGS find that the temperature depends mainly on the chemistry of hydrogen and not on the

heavy elements. In principle, the dynamical, thermal, and chemical properties of the wind should be obtained in a completely self-consistent calculation. The complexity of the chemical considerations to be described below and the two-dimensional nature of the hydrodynamics indicate that such calculations would be extremely difficult, if not infeasible, at the present time.

The primary objective of this paper is to describe the physical and chemical considerations that apply in low-luminosity protostellar winds. We illustrate the role of the most important processes with simplified models, especially those suggested by protostellar theory (RGS). In order to develop a basis for applications to other models, we vary the wind parameters and consider particular modifications in the basic model such as the effects of far-UV radiation, which might arise, for example, from an accretion shock. Our results provide insights into the physical conditions that are required for efficient molecular synthesis and on potential molecular diagnostics of protostellar winds.

The organization of the paper is as follows. Section 2 gives a full description of the dynamical model and the underlying physical and chemical processes, including radiation transport. Section 3 presents the results of the calculations, and § 4 summarizes the main conclusions, particularly those relevant to observational studies. The reader interested primarily in the results may wish to first read § 2.1, where the basic models are described, and then skip to § 3.

### 2. THE MODEL

#### 2.1. The Physical Model

We represent the primary wind of a low-luminosity protostar by a steady, spherical flow with density, velocity, and temperature fields,  $n(r)$ ,  $v(r)$ , and  $T(r)$ , all *specified* functions of the radial distance  $r$  from the center of the protostar. Our objective is to calculate the ionization and the chemical abundances with these functions as “given.” This separation of the chemistry from the hydrodynamics is justified in practical terms, i.e., the

<sup>1</sup> Permanent address: DAEC, Observatoire de Meudon, 92195 Meudon Principal Cedex, France.

full problem is too complex. A similar justification underlies the use of one-dimensional flows. However, here we invoke the device of an “equivalent, quasi-spherical” flow (RGS) that incorporates the most important effect of wind collimation, which is to increase the density of the wind near the protostar.

The density  $n(r)$  is defined as the volume density of hydrogen nuclei in all species. The velocity is represented as

$$v = u(r)V, \quad (1)$$

where  $V$  is the terminal speed of the wind and  $u$  describes its acceleration; usually  $u < 1$ . We assume steady flow and, following RGS, allow for the possibility that, at a distance  $r$ , the wind crosses an area  $4\pi r^2 A(r)$ , with  $A < 1$ , i.e., only a fraction  $A$  of the allowed area. Thus the density  $n(r)$  is determined directly by mass conservation and is parametrized by the hydrogen mass-loss rate  $\dot{M}$  as follows:

$$n(r) = (\dot{M}/4\pi r^2 mV)(1/uA). \quad (2)$$

In practice we mainly consider three flow cases:

$$\text{Case 1: } A = 1, u = 1, \quad (3a)$$

$$\text{Case 2: } A = 1, u = 1 - R_*/r, \quad (3b)$$

$$\text{Case 3: } A = 1 - R_*/r, u = 1 - R_*/r. \quad (3c)$$

In Case 1, the flow is started “impulsively” at the stellar radius ( $R_*$ ) and emerges isotropically; this is the flow assumed in Paper I. Case 2 is more realistic than Case 1 in that the terminal speed is reached over a finite distance of the order of the stellar radius; the flow is still everywhere isotropic. In Case 3, the flow emerges from an infinitesimal (equatorial) region and becomes isotropic at large distances; this case is actually RGS Case 4. The singularities in Case 2 and Case 3 are avoided by starting the integration at the sonic point, as discussed by RGS. The function  $1 - R_*/r$  then varies from  $a/V$  to 1, where  $a$  is the sound speed at  $R_*$  and  $a \ll V$ .

In accord with observations and theory for protostars, (see, for example, the review of Shu et al. 1987 or RGS), typical parameters for low-luminosity protostars are  $T_* = 3500\text{--}6500$  K,  $R_* = 5 \times 10^{11}\text{--}3 \times 10^{12}$  cm, and  $\dot{M} = 10^{-7}\text{--}10^{-5} M_\odot \text{ yr}^{-1}$ . We adopt a “standard” set of parameters suggested by the observationally important protostellar source SSV 13, associated with HH 7–11:  $T_* = 5000$  K,  $R_* = 6.63 \times 10^{11}$  cm,  $\dot{M} = 3 \times 10^{-6} M_\odot \text{ yr}^{-1}$ ; the luminosity is about  $50 L_\odot$ . For this set, equation (3) becomes

$$n(r) = 2.4 \times 10^{12} (R_*/r)^2 (1/uA) \text{ cm}^{-3}, \quad (4)$$

and  $V/a = 22$ . In going from Case 1 to Case 3, the density close to the protostar increases by  $(V/a)^2 = 466$  for these parameters and is greater than  $10^{15} \text{ cm}^{-3}$  for Case 3.

Figure 1 shows the RGS temperature distributions for  $\dot{M} = 3 \times 10^{-6} M_\odot \text{ yr}^{-1}$ . For comparison, we show the ad hoc form introduced in Paper I,

$$\begin{aligned} T &= T_0 & r < R_0, \\ T &= T_0 (R_0/r)^p & r > R_0, \end{aligned} \quad (5)$$

for the choice  $p = -4/3$ ,  $T_0 = 5000$  K, and  $R_0 = 2R_*$ . The RGS distribution for Case 1 has a modest increase at large  $r$ , relative to the adiabatic distribution ( $T = T_* r^{-4/3}$ ), due to ambipolar diffusion heating. For Cases 2 and 3, the temperature drops very rapidly at first because of enhanced adiabatic cooling, but then  $\text{H}_2$  formation heating and ambipolar diffusion heating reverse this trend. Ambipolar diffusion

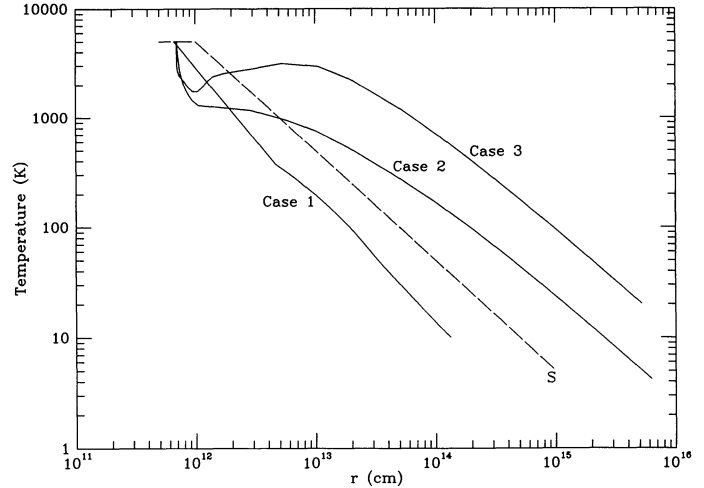


FIG. 1.—Temperature distributions corresponding to the RGS cases defined by equation (3) and  $\dot{M} = 3 \times 10^{-6} M_\odot \text{ yr}^{-1}$ . The dashed curve, labeled S, is the temperature model used in Paper I.

heating is responsible for keeping the gas warm at large distances and, in Case 3, reheats the gas to 3000 K, high enough to destroy  $\text{H}_2$ , but not CO, by collisional dissociation.

Another physical property important for the molecular physics of the wind is the radiation field. We assume that the only source of radiation is the protostar, which we treat as a blackbody with (photospheric) temperature  $T_*$ . At a distance  $r$ , radiative rates are reduced by the standard dilution factor,

$$W(r) = 1/2[1 - (1 - R_*^2/r^2)^{1/2}] \quad (6)$$

and by absorption by various species. We shall take up the calculation of radiative transfer in the wind in § 2.3 and departures from a blackbody in § 3.4.

## 2.2. Chemistry and Ionization

We describe the calculation of the chemical abundances in the wind, assuming that the wind flows from the protostar in the manner described in § 2.1. Electrical neutrality is assumed so that the electron density  $n_e$  is the difference between the densities of positive and negative ions. The short dynamical time scale of the flow, typically

$$t_{dy} = r/v \approx 10^5 (r_{12}/v_7) \text{ s} \quad (7)$$

( $r_{12} = r/10^{12}$  cm and  $v_7 = v/10^7$  cm s $^{-1}$ ), means that kinetic rather than steady state chemistry is required. Thus the rate equation for species  $Y$  has the generic form

$$v d/dr x(Y) = P(Y) - D(Y)x(Y) \quad (8)$$

where  $P$  and  $D$  are appropriate production and destruction rates. The initial conditions are calculated for steady state photospheric physical conditions using standard cosmic abundances. Our program reads the input set of chemical reactions and rate coefficients and internally derives the rate equations for each species. The system of rate equations is integrated using Gear’s (1971) method for stiff, ordinary differential equations. The integration is performed for the abundances as a function of  $\log r$ , starting at the stellar surface and integrating outwards. The calculations typically require about 20 minutes of CPU time on a Convex C210 mini-supercomputer.

For the flows in equation (3), the hydrogen density  $n$  ranges up to  $10^{15} \text{ cm}^{-3}$  and the temperature  $T$  up to 5000 K or more.

Although  $n$  and  $T$  decrease rapidly with distance, their values in chemically active regions are considerably higher than encountered in interstellar clouds away from star-forming regions. The radiation field and velocity gradient (essentially the inverse of  $t_{dy}$  in equation [7]) are also much greater. Thus protostellar wind chemistry involves relatively extreme physical conditions and differs from familiar interstellar chemistry. There are interesting connections with the chemistry of the early universe (Dalgarno & Lepp 1987), with the reformation of molecules behind shocks (Neufeld & Dalgarno 1989a, b), and with the formation of molecules in supernova shells (Lepp, Dalgarno, & McCray 1990; Petuchowski et al. 1989). In the following subsections, we describe the essential aspects of our chemical model. Although the chemistry is reasonably complete, we have had to be judicious in the selection of the included processes because of the heavy computational demands of the radiation transfer.

### 2.2.1. Three-Stage Synthesis of Heavy Molecules

We start with an overview of the chemistry and consider the synthesis of CO, one of the most important molecular diagnostics. Figure 2 is a greatly simplified schematic diagram of the three-stage synthesis of CO described briefly in Paper I. Because the wind is hydrogen-rich and the density and temperature are high, the first step toward molecular synthesis is the formation of  $H_2$ , which can be achieved in three ways, which we refer to as the  $H^-$ ,  $H_2^+$ , and three-body routes. The first two dominate for Case 1 (unless  $\dot{M} > 10^{-4} M_\odot \text{ yr}^{-1}$ ) whereas the densities in Cases 2 and 3 are sufficiently high for three-body formation to dominate (unless  $\dot{M} < 10^{-7} M_\odot \text{ yr}^{-1}$ ). In addition to the three progenitor reactions, the full hydrogen chemistry includes reactions that neutralize  $H^-$  and  $H_2^+$ , that ionize  $H$ , and a variety of photo processes to be discussed in § 2.2.3. The ionization of atomic hydrogen occurs by collisional excitation of the  $n = 2$  level followed by photoionization from this level by Balmer continuum radiation. The main destruction mechanisms for  $H^+$  are radiative recombination and charge exchange. We forego an extensive discussion of the hydrogen chemistry (other than photo processes) because it is described in full detail in RGS.

Once  $H_2$  is formed, neutral reactions with atomic oxygen produce OH if the wind is warm (the energy barrier is 3940 K) and then CO by reaction of OH with atomic carbon (without any significant energy barrier). A similar three-stage pathway with CH is also shown in Figure 2; it is less effective because of the larger barrier for the formation of CH. Also illustrated in

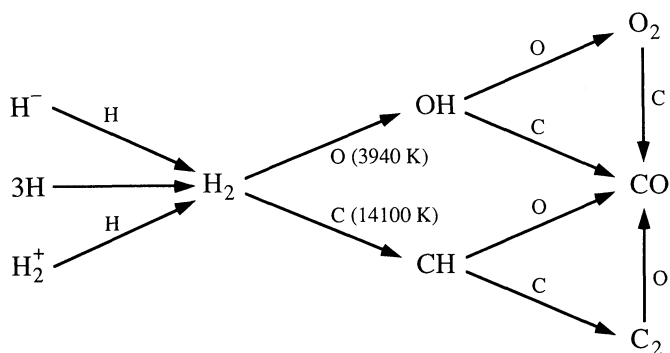


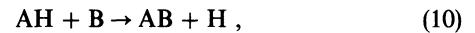
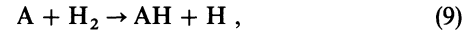
FIG. 2.—Three-stage synthesis of heavy molecules. The numbers under the dashed arrows give the energy barriers for the endothermic reactions,  $O + H_2 \rightarrow OH + H$  (3940 K) and  $C + H_2 \rightarrow CH + H$  (14,100 K).

Figure 2 are the fourth-stage molecules  $O_2$  and  $C_2$ , each of which can lead to CO by another neutral reaction.

Under appropriate circumstances, molecules can also be formed by ion-molecule reactions and by radiative association (for diatomic species). Destruction routes are also critical and we have considered a wide range of processes that include neutral and ionic reactions, collisional dissociation, charge exchange, photoionization and photodissociation, and recombination and neutralization of ions. In the following, we discuss the roles of the different reactions and how we obtained their rate coefficients.

### 2.2.2. Neutral Reactions

The schematic chemistry in Figure 2 indicates the type of neutral reactions that are important in protostellar winds:



where  $A, B = O, C, N, S,$  and  $Si$ . The level of laboratory and theoretical information on these types of reactions is mixed, with rather reliable data for reactions of  $O, C,$  and  $S$  (at and just above  $T = 300$  K) and considerably less for  $N$  and  $Si$ . We rely primarily on the compilations of Baulch et al. (1984) and on the recent theoretical work of Graff and collaborators (Wagner & Graff 1987; Graff & Dalgarno 1987; Leen & Graff 1988; Graff 1989). Even with limited data, some general trends are readily discernible within the set of atoms that we consider. The most important factor is the relatively small energy barrier of the  $O + H_2 \rightarrow OH + H$  reaction, which means that reaction (9) leads to the production of much more OH than any other hydride. By contrast,  $O, C, N,$  and  $S$  all are known to engage readily with OH in reaction (10);  $Si$  probably does too, although the rate coefficient has not been measured. The important conclusion here is that OH can be effectively formed from  $H_2$  by reaction (9) and that essentially all of the heavy oxides can be synthesized from OH with reaction (10).

The primary role of three-body, neutral reactions is the synthesis of  $H_2$  (Paper I; RGS). The inverse process of collisional dissociation is potentially important for  $H_2$  and other molecules with vanishing or small dipole moments, notably CO and the homonuclear molecules  $C_2, N_2,$  and  $O_2$ . This process only occurs rapidly from excited vibrational levels and the rate coefficient  $k_d$  is negligible unless the density exceeds some critical value  $n_{cr}$  (Roberge & Dalgarno 1982). For  $H_2, n_{cr} \approx 10^5 \text{ cm}^{-3}$  (Lepp & Shull 1983), but it is much larger for CO,  $\approx 10^{11} \text{ cm}^{-3}$  (Roberge & Dalgarno 1982). For  $n > n_{cr}, k_d$  goes over to the high-density, thermal equilibrium limit, presumably also characteristic of laboratory measurements (when they exist).

In practice we use the experimental values for  $H_2$  recommended in the critical review of Cohen & Westburg (1983). We ignore the density dependence of the rate coefficients because  $n \gg n_{cr}$  in the chemically active regions of protostellar winds. Furthermore,  $k_d$  has a temperature barrier of about 53,000 K in this case, which cuts in before the dependence associated with  $n/n_{cr}$ . In the absence of any information on the collisional dissociation rates of other homonuclear molecules, we use the same rates as for  $H_2$  but with barriers determined by the dissociation energies. For CO, we use the high-density theoretical calculation of Roberge & Dalgarno (1982) whenever the initial density is greater than  $10^{11} \text{ cm}^{-3}$ . The large temperature barrier ( $\approx 97,000$  K) helps to suppress the effect of CO collisional dissociation as does destruction by the chemical reaction,  $H + CO \rightarrow OH + C$ , which has a barrier of 77,500 K.

Similar reactions play an even more important role in destroying  $O_2$ ,  $C_2$ , and  $N_2$  because of the smaller energy barriers. Our approximate treatment of CO collisional dissociation overestimates its effect in cases where the density in the region of CO formation is about the same as the critical density. For example, in Case 1 for the standard mass-loss rate, our calculation of the freeze-out abundance of CO may be too small by a factor of 2 because we ignore the cutoff of this process for  $n < n_{cr}$ .

### 2.2.3. Ionic Reactions

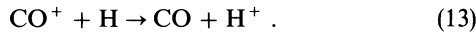
Ion-molecule reactions familiar in interstellar chemistry supplement molecular synthesis in protostellar winds that do not recombine strongly. The primary ions in such winds are atomic rather than molecular and they are produced by the protostellar radiation field. Although  $H_2^+$  is important in the synthesis of  $H_2$ , its abundance is generally quite small (usually  $< 10^{-10}$ ). Consequently only a small amount of  $H_3^+$  is made by the reaction



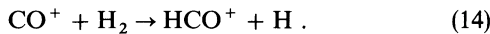
A more important molecular ion is  $CO^+$ , which is produced by



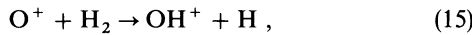
and produces CO by charge exchange with atomic hydrogen



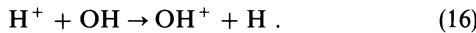
Some  $HCO^+$  is formed by the reaction



The most abundant molecular ion after  $H_2^+$  is generally  $OH^+$ , which is formed by the ion-molecule reaction



and, somewhat more efficiently, by charge-exchange



Where there are enough ions for these processes to be interesting, the  $H_2$  abundance is too small to make much  $H_2O^+$  and the  $OH^+$  is destroyed by dissociative recombination, which is a very rapid process for the ionization levels characteristic of these winds. Thus reaction (15) fails to lead to heavy-molecule synthesis, and reaction (16) effectively destroys  $OH$ . This conclusion applies fairly generally because  $H^+$  is able to charge-exchange with many molecules.

In addition to charge exchange with molecules (which leads to their destruction by dissociative recombination following charge exchange), purely atomic charge exchange



is crucial for the correct calculation of the ionization of the wind. Only a few of the relevant charge-exchange rate coefficients have been measured or even studied theoretically in any detail. In the absence of any better information, we rely on the educated theoretical guesses of Pequignot & Aldrovandi (1986). We list the charge-exchange reactions in Table 1; the energy barriers for the reverse reactions are taken as the differences in the ionization potentials. The most important charge exchange reactions are  $H^+$  with O and Fe for which, fortunately, some experimental results exist. For the  $H^+ + O$  rate coefficient, we use the theoretical temperature variation of Chambaud et al. (1980) which agrees with the room temperature measurement of Fehsenfeld & Ferguson (1972). The

TABLE 1  
ATOMIC CHARGE-EXCHANGE CHART<sup>a</sup>

ION	ATOM							
	H	C	S	Si	Fe	Mg	Al	Na
$O^+$	0.18 <sup>b</sup>	0	0	0	2.9 <sup>b</sup>	0	0	0
$H^+$		0	3	0	7.4 <sup>c</sup>	0 <sup>d</sup>	3	0
$C^+$			0	1	3	0	0.3	0
$S^+$					3	0	0	0
$Si^+$					3	1	3	0
$Fe^+$						3	1	3
$Mg^+$							0	0
$Al^+$								0

<sup>a</sup> Units for rate coefficients are  $10^{-9} \text{ cm}^3 \text{ s}^{-1}$ .

<sup>b</sup> Measured value for  $H^+ + O$  at 300 K (Fehsenfeld & Ferguson 1972) supplemented by theory (Chambaud et al. 1980) at other temperatures.

<sup>c</sup> Measured value at  $T = 300 \text{ K}$  (Rutherford & Vroom 1972).

<sup>d</sup> We use the theoretical result of Allan et al. (1988),  $1.25 \times 10^{-9} \exp(-22,100 \text{ K}/T)$ .

$H^+ + Fe$  charge exchange cross section was measured at high energies (more than 8 eV) by Rutherford & Vroom (1972) and extrapolated by them to much lower energies using theory; we use their  $T^{-0.5}$  dependence for  $T < 5000 \text{ K}$ . Charge-exchange greatly reduces the abundance of  $H^+$  and causes the ionization to be transferred to heavier atomic ions which can survive longer in the wind. This tendency is assisted by the reduction in the shielding of various ionizing continua that results from the ionization of the atoms. Charge-exchange ensures that the ionization level remains moderately high even for high-density winds.

### 2.2.4. Radiative Reactions

Two-body association accompanied by the emission of radiation can form heavy molecules as well as the progenitor species  $H^-$  and  $H_2^+$  (paper I; RGS). Although the characteristic rate coefficients are small,  $\approx 10^{-18} - 10^{-17} \text{ cm}^3 \text{ s}^{-1}$ , this process can be effective in the cooler parts of the wind where other production mechanisms are shut off. We list the radiative association reactions in Table 2. Radiative recombination of electrons and ions is a much better studied process, and the rates we adopt are similar to those used by others.

### 2.3. Photoprocesses

Ultraviolet photons from the protostar ionize the atoms and dissociate the molecules of the wind. Because we are concerned with very young, highly embedded protostars, we neglect the interstellar radiation field and Galactic cosmic rays. Table 3 lists the photoprocesses that we consider and the sources for the cross sections, which are mainly for the ground state of the

TABLE 2  
ATOMIC RADIATIVE ASSOCIATION RATES

System	Rate ( $\text{cm}^{-3} \text{ s}^{-1}$ )	Reference
$O + H$ .....	6.2(-19)	Smith & Zweibel (1976)
$C + H$ .....	1.5(-18)	Brooks & Smith (1974)
$Si + H$ .....	1.5(-19)	Adapted from carbon
$C^+ + H$ .....	1.7(-17)	Graff et al. (1983)
$C + O$ .....	2.6(-17) $\exp(-1450 \text{ K}/T)$	Dalgarno, Du, & Yu (1990)
$C^+ + O$ .....	2(-18)	Dalgarno, Du, & Yu (1990)
$Si + O$ .....	2(-17)	Adapted from carbon
$Si^+ + O$ .....	2(-18)	Adapted from carbon

TABLE 3  
PHOTO RATES<sup>a</sup>

Reaction	Typical Rate	Reference
H ( $n = 2$ ) $\rightarrow$ H <sup>+</sup> .....	3.63 (3)	Karzus & Latter (1961)
H <sup>-</sup> $\rightarrow$ H + $e$ .....	5.21 (5)	Wishart (1979)
H <sub>2</sub> <sup>+</sup> $\rightarrow$ H <sup>+</sup> + H .....	3.87 (3)	Argyros (1974)
H <sub>2</sub> $\rightarrow$ H + H .....	2.10 (-5)	Stephens & Dalgarno (1972)
CO $\rightarrow$ C + O .....	5.43 (-4)	Letzelter et al. (1987)
SiO $\rightarrow$ Si + O .....	0.470	Adapted from CO
OH $\rightarrow$ O + H .....	0.442	van Dishoeck & Dalgarno (1984)
H <sub>2</sub> O $\rightarrow$ OH + O .....	2.04	Hudson (1971); Lee (1984)
O <sub>2</sub> $\rightarrow$ O + O .....	0.819	Black & Smith (1984)
CH $\rightarrow$ C + H .....	16.4	van Dishoeck (1987)
C <sub>2</sub> $\rightarrow$ C + C .....	1.74 (-4)	Pouilly et al. (1983)
C ( $n = 1$ ) $\rightarrow$ C <sup>+</sup> + $e$ ....	4.89 (-4)	Escalante & Victor (1990)
C ( $n = 2$ ) $\rightarrow$ C <sup>+</sup> + $e$ ....	7.90 (-3)	Escalante & Victor (1990)
C ( $n = 3$ ) $\rightarrow$ C <sup>+</sup> + $e$ ....	1.88 (-2)	Escalante & Victor (1990)
C ( $n = 4$ ) $\rightarrow$ C <sup>+</sup> + $e$ ....	4.66	Escalante & Victor (1990)
Si $\rightarrow$ Si <sup>+</sup> + $e$ .....	0.993	Hudson & Kieffer (1971)
S $\rightarrow$ S <sup>+</sup> + $e$ .....	2.69 (-2)	Tondello (1972)
Mg $\rightarrow$ Mg <sup>+</sup> + $e$ .....	9.98 (-2)	Hudson & Kieffer (1971)
Fe $\rightarrow$ Fe <sup>+</sup> + $e$ .....	0.184	Kelly & Ron (1972)
Al $\rightarrow$ Al <sup>+</sup> + $e$ .....	1.07 (2)	Roig (1975)
Na $\rightarrow$ Na <sup>+</sup> + $e$ .....	0.905	Hudson & Kieffer (1971)

<sup>a</sup> At  $1.05R_*$  for a  $T_* = 5000$  K blackbody; units are  $s^{-1}$ .

species and are well established. The third column of Table 3 gives the rate at the photosphere ( $R_*$ ) for  $T_* = 5000$  K.

Because photoreactions often dominate the ionization of these winds, it is important to treat the transfer of the UV radiation self-consistently. Stellar photons can be absorbed and scattered by atoms and molecules and by dust grains. The corresponding cross sections generally depend on wavelength and a wavelength-dependent treatment of the radiative transfer is called for. In our model, we divide the UV spectrum into a finite number  $N_{\text{abs}}$  of bands and calculate averages over the photoabsorption cross section for each species in each band. For this purpose, we tabulate the cross sections referred to in Table 3 and fit them with cubic-splines in log-log space for greater accuracy. When necessary, the tabular data is extrapolated assuming a constant slope in log-log space.

Our program allows for the incorporation of dust opacity although we have not included it in the present calculations. RGS did consider the possibility that dust might heat the gas and found that it had little effect. The formation of dust could have some chemical consequences at distances from the protostar of the order of  $10R_*$ , e.g., it could increase the UV opacity for wavelengths where the atoms are ineffective. Dust might also reduce the ionization of the outer wind by neutralizing the atomic ions that are the dominant source of ionization far from the protostar. We have chosen not to include dust formation at this time because it mainly forms outside the region of rapid molecule formation.

The unshielded photorates are computed from cross sections by integration with the spectral distribution of the flux, most often a blackbody spectrum. Labeling the wavelength bands by  $k$ , the photorate for species  $j$  at a distance  $r$  from the protostar is

$$g_j(r) = W(r) \sum_k g_{j,k}^{(0)} \exp[-\tau_k(r)], \quad (18)$$

where  $W$  is the dilution factor of equation (6) and  $g_{j,k}^{(0)}$  is the unshielded rate evaluated at the photosphere; the optical

depth for band  $k$  is a sum over species  $j$ :

$$\tau_k(r) = \sum_j \tau_{j,k}(r), \quad (19)$$

$$\tau_{j,k}(r) = \int_{R_*}^r dr' x_j n(r) \sigma_{j,k}, \quad (20)$$

where  $\sigma_{j,k}$  is the average absorption cross-section of species  $j$  in wavelength band  $k$ .

In principle, the calculation of photorates should take into account the population of excited states. Because of the large computational demands of such calculations in a chemical kinetics program, we generally assume that photodestruction occurs from the ground state, with three exceptions: H, C, and H<sub>2</sub>. For atomic hydrogen, most of the photoionization occurs from the first excited level, so we include both the  $n = 1$  and  $n = 2$  levels (Paper I, RGS). Atomic carbon is the single most important far-UV shielding species and we include photoionization from and recombination to its first three excited electronic levels as well as the ground level. We calculate the population of the levels in a fully kinetic manner, including collisional excitation and de-excitation and chemical reactions as well as the radiative processes just mentioned.

Photodissociation of thermally equilibrated H<sub>2</sub><sup>+</sup> occurs from a large number of excited vibrational levels. Because of the small Einstein  $A$ -values, thermal equilibrium is a good approximation in the inner wind where the peak abundances of H<sub>2</sub><sup>+</sup> occur. We have tabulated the thermally averaged cross sections of Argyros (1974) as a function of wavelength and temperature, and have fit log-log cubic splines to these data, extrapolating with a constant slope in log-log space when necessary. The photorates are computed by integrating out to  $36,000 \text{ \AA}$ , which yields an accuracy typically better than 5%. Photodissociation is the most important destruction mechanism for H<sub>2</sub><sup>+</sup> and it is not suppressed very significantly by shielding by other species as are most other molecules. For a protostar with a 5000 K blackbody spectrum, the photodestruction time scale for H<sub>2</sub><sup>+</sup> in gas with a kinetic temperature of 5000 K is  $10^{-3}$  s.

The calculation of the shielding of the ionizing and dissociating radiation is done self-consistently using the method of Mamon, Glassgold, & Omont (1987) where the differential form of equation (20) is integrated for each band simultaneously with the chemical rate equations. If  $N_{\text{abs}}$  is the number of absorbers,  $l_{\text{max}}$  the number of bands, and  $N_{\text{sp}}$  the number of chemical species, then altogether we integrate  $N_{\text{sp}} + l_{\text{max}} N_{\text{abs}}$  equations, or about 250 in practice. For purposes of simplicity, we treat all molecular shielding as a continuum process. Although H<sub>2</sub> and CO photodissociation occur through lines, our approximation makes little difference because the relevant 900–1000  $\text{\AA}$  wavelength band is so heavily blocked by atomic absorption, especially by carbon and sulfur.

### 3. RESULTS

In this section we present results for the models introduced in § 2. The three cases defined in equation (3) represent a sequence of increasing physical complexity and, presumably, of increasing realism in modeling very young, low-mass protostars. For each case we calculate the abundances for mass-loss rates,  $\dot{M} = 3 \times 10^{-7}$ ,  $3 \times 10^{-6}$ , and  $3 \times 10^{-5} M_{\odot} \text{ yr}^{-1}$ . Because the three cases differ in their velocity and temperature fields, the grid of nine basic calculations provide a good idea of how the results depend on the most important physical variables: temperature, density, and flow velocity. The asymptotic

TABLE 4  
 ASYMPTOTIC ABUNDANCES

$\dot{M}$	CASE 1			CASE 2			CASE 3		
	3 (-7)	3 (-6) ( $M_{\odot} \text{ yr}^{-1}$ )	3 (-5)	3 (-7)	3 (-6) ( $M_{\odot} \text{ yr}^{-1}$ )	3 (-5)	3 (-7)	3 (-6) ( $M_{\odot} \text{ yr}^{-1}$ )	3 (-5)
H	1.0	1.0	0.99	1.0	1.0	0.72	1.0	1.0	0.18
H <sub>2</sub>	5.0-6	2.1-6	5.2-3	1.1-5	1.5-3	1.4-1	3.5-7	8.2-6	4.1-1
x <sub>e</sub>	1.4-4	7.5-5	5.5-6	1.2-4	4.3-5	7.0-6	2.8-4	8.5-5	7.3-6
C	4.0-4	4.0-4	0	3.9-4	0	0	3.8-4	8.5-12	0
C <sup>+</sup>	3.8-11	0	0	1.1-11	0	0	2.8-5	0	0
CO	2.8-7	7.9-6	4.0-4	1.1-5	4.0-4	4.0-4	5.9-7	4.0-4	4.0-4
CH	7.0-12	7.2-11	0	6.8-12	0	0	6.7-12	2.9-18	0
C <sub>2</sub>	3.1-12	3.6-11	0	3.4-12	0	0	1.9-12	0	0
O	8.0-4	7.9-4	1.6-4	7.9-4	3.6-4	2.2-8	8.0-4	3.8-4	4.4-11
OH	2.2-10	4.1-9	2.6-8	2.2-10	7.3-9	2.6-12	2.2-10	1.1-8	1.3-15
H <sub>2</sub> O	0	0	8.2-5	0	6.8-19	3.6-4	0	7.0-12	3.6-4
O <sub>2</sub>	4.2-16	2.3-11	5.8-5	1.5-12	9.1-8	6.6-10	2.4-12	6.7-8	3.1-12
Si	1.2-7	2.6-5	0	3.0-8	5.2-16	0	2.4-8	1.3-5	0
Si <sup>+</sup>	3.7-5	1.1-5	0	3.7-5	0	0	3.8-5	7.4-6	0
SiO	2.2-14	3.7-10	3.8-5	2.4-14	3.8-5	3.8-5	3.8-15	1.7-5	3.8-5
S <sup>+</sup>	1.6-5	0	0	3.8-10	0	0	1.8-6	3.4-10	0
Mg <sup>+</sup>	3.8-5	3.6-5	6.0-9	4.0-5	3.7-5	4.6-6	4.0-5	4.0-5	4.9-6
Fe <sup>+</sup>	3.3-5	2.2-5	0	3.4-5	2.5-7	0	3.4-5	3.3-5	0
Al <sup>+</sup>	3.2-6	3.2-6	3.2-6	3.2-6	3.2-6	9.1-8	3.2-6	3.2-6	9.6-8
Na <sup>+</sup>	2.3-6	2.3-6	2.3-6	2.3-6	2.3-6	2.3-6	2.3-6	2.3-6	2.3-6

abundances of representative species for these models are summarized in Table 4. In § 3.4, we investigate the effects of varying the radiation field.

### 3.1. Case 1: Isotropic, Impulsive Wind

Case 1 is similar to the model discussed in Paper I. The wind expands isotropically at constant velocity and the temperature decreases monotonically with distance. The relatively small departures from an adiabatic fall-off calculated by RGS have little effect on the chemistry because they occur at large distances where the chemistry is frozen out. For Case 1 and  $\dot{M} = 3 \times 10^{-6} M_{\odot} \text{ yr}^{-1}$ , Figure 3 illustrates the radial variation in the wind of the abundances of representative species. Compared with the corresponding Figure 1 of Paper I, the abundances of H<sub>2</sub> and CO are about the same order of magnitude,  $10^{-5}$ , but now the abundance of SiO is much smaller due to the implementation of a full rather than the earlier, schematic silicon chemistry. Another major difference is the rapid decline in the abundance of H<sup>+</sup> at  $2R_{*}$  due to the inclusion of many more charge exchange reactions. The abundances of the  $n = 2$  level of hydrogen and H<sub>2</sub><sup>+</sup> (which are not shown) also decrease rapidly. The bulk of the carbon is atomic throughout the wind and S<sup>+</sup>, which is produced by charge-exchange of H<sup>+</sup> and S, recombines as soon as H<sup>+</sup> disappears. Among the other heavy ions, only Si<sup>+</sup> recombines completely (by  $200R_{*}$ ) so that the electron fraction is of order  $10^{-4}$  throughout much of the envelope. The asymptotic values of many of the calculated abundances are given in the third column of Table 4. The substantial asymptotic abundances of the radical hydrides, OH and CH, and of the molecules synthesized from them are due to radiative association.

Figure 3 describes a wind that is still basically atomic; the density for  $\dot{M} = 3 \times 10^{-6} M_{\odot} \text{ yr}^{-1}$  is too small to produce short chemical time scales, and the chemistry is incompletely developed. Although the asymptotic fraction of carbon atoms in molecules (0.02) is small, it is much larger than that of hydrogen ( $4 \times 10^{-5}$ ). This difference reflects primarily the difference in binding energy between CO and H<sub>2</sub>. For the tem-

perature range expected for young, low-mass, protostellar winds (RGS), collisional dissociation of CO is much more strongly suppressed than for H<sub>2</sub>. Table 4 shows the sensitive dependence of the chemistry on the mass-loss rate; the degree

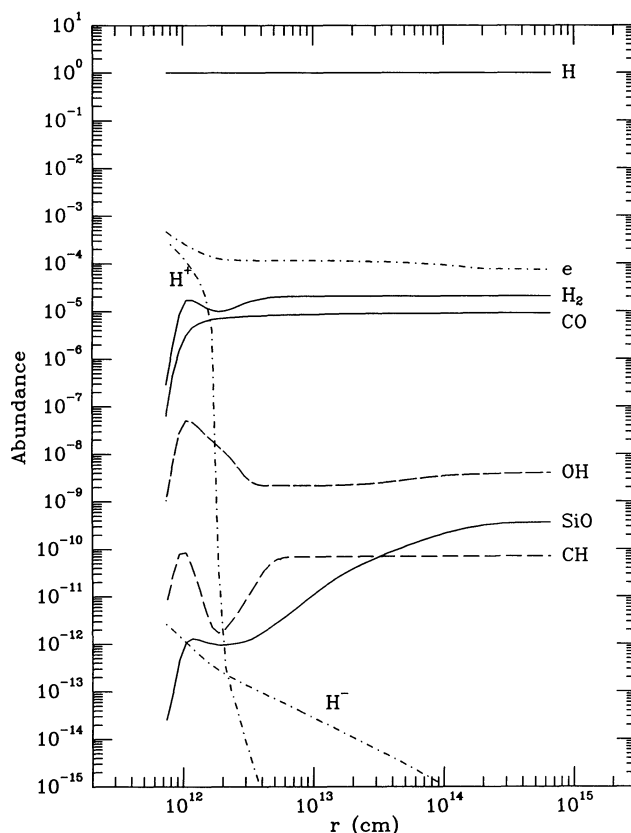


FIG. 3.—Chemical abundances for Case 1 and  $\dot{M} = 3 \times 10^{-6} M_{\odot} \text{ yr}^{-1}$ . Ionic abundances are represented by dot-dashed lines; the solid and dashed lines are used to distinguish the neutral species.

of molecular synthesis is smaller for the lower mass-loss rate,  $\dot{M} = 3 \times 10^{-7} M_{\odot} \text{ yr}^{-1}$  [ $x(\text{CO})/x_{\text{C}} \rightarrow 7.5 \times 10^{-4}$ ], but, for  $\dot{M} = 3 \times 10^{-5} M_{\odot} \text{ yr}^{-1}$ , it is almost complete for CO and SiO. For the highest mass-loss rate, none of the carbon or silicon is left in atoms or radicals at large distances, whereas only 0.005 of the hydrogen is in  $\text{H}_2$ , i.e., the wind is still atomic from the point of view of hydrogen. The situation with oxygen is different, in that the residual oxygen left over from the synthesis of CO is divided among O and  $\text{H}_2\text{O}$  but a significant amount remains in OH [ $x(\text{OH}) \simeq 4 \times 10^{-8}$ ]. The extent to which any oxygen is outside of  $\text{H}_2\text{O}$  measures the incompleteness in the chemical evolution. The ionization fraction is significantly reduced in this case (the highest mass-loss rate,  $3 \times 10^{-5} M_{\odot} \text{ yr}^{-1}$ ) because all of the heavy ions except  $\text{Al}^+$  and  $\text{Na}^+$  recombine. These ions are the most resistant to recombination because the corresponding thresholds for atomic photoionization occur at long wavelengths (beyond 2000 Å) where the protostellar flux is relatively large and where other, more abundant atoms, cannot shield the ionizing radiation.

### 3.2. Case 2: Isotropic, Accelerated Wind

This model is more realistic than Case 1 in that it includes wind acceleration. The most important consequences for the chemistry are that the dynamical time scale and the density are each increased by a factor of  $V/a$  at the base of the wind (where  $V$  = terminal speed and  $a$  = sound speed), which is a factor of 22 in these calculations. Because the chemical time scale is decreased and the dynamical time increased by this same factor, molecular synthesis is much more efficient than in Case 1 for the same mass-loss rate. The temperature distribution also changes so there is some potential for lower molecular abundances because the temperature is generally higher than in Case 1. However, the RGS temperature distributions are all monotonically decreasing for this case and, most important, fall even more rapidly near the protostar than in Case 1. Thus, relative to Case 1, the density increase dominates the changes in the chemistry because the photoprocesses remain at about the same rate.

As can be seen from Table 4, the CO abundance reaches a substantial level,  $\approx 10^{-5}$ , for the lowest mass-loss rate,  $\dot{M} = 3 \times 10^{-7} M_{\odot} \text{ yr}^{-1}$ , but the abundances of all the other molecules are low. This calculation illustrates again how a poorly collimated wind with a modest mass-loss rate can be essentially atomic and moderately ionized ( $x_e \approx 10^{-4}$ ) but still have CO as the only molecule with a substantial abundance. Once the mass-loss rate reaches  $\dot{M} = 3 \times 10^{-6} M_{\odot} \text{ yr}^{-1}$ , however, all of the available carbon and silicon are in CO and SiO, as shown in Figure 4. Most of the residual oxygen is in O and there is also some in OH, but there is very little in  $\text{O}_2$  and  $\text{H}_2\text{O}$  which, under these conditions, are unable to compete with CO and SiO for oxygen. The ionization level is moderate because several ions are unrecombined, as given in Table 4. For  $\dot{M} = 3 \times 10^{-5} M_{\odot} \text{ yr}^{-1}$ , illustrated in Figure 5, essentially all of the heavy molecules are processed into their most stable forms. There are few radicals and the ionization level is small, again with only  $\text{Al}^+$  and  $\text{Na}^+$  unrecombined. It is interesting that the fraction of protons frozen out in  $\text{H}_2$  is still only 30% for this mass-loss rate. The large abundance of molecular hydrogen is due to three-body formation, which dominates the other two formation channels (see Fig. 2) because the density close to the protostar is very large,  $\approx 10^{14} \text{ cm}^{-3}$ . Ion-molecule reactions are now unimportant in the synthesis of the heavier molecules.

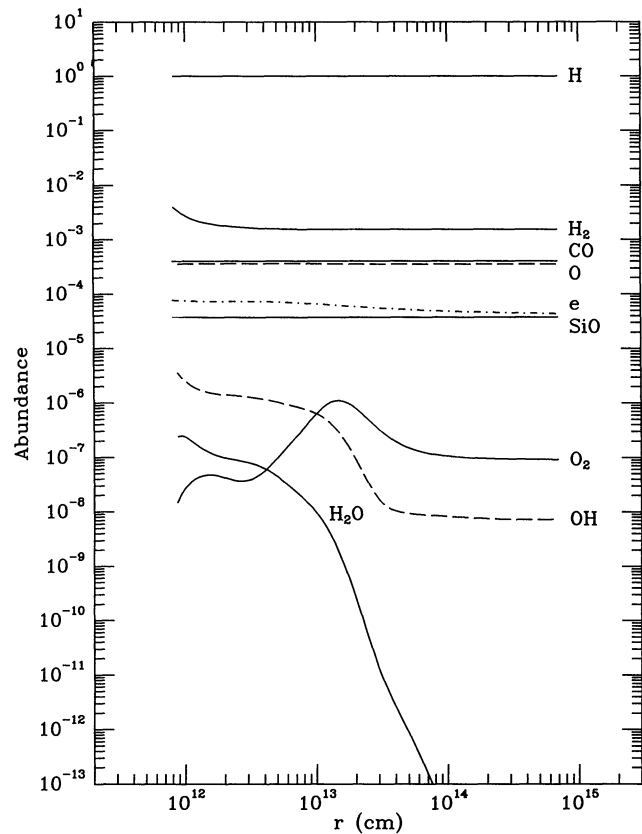


FIG. 4.—Chemical abundances for Case 2 and  $\dot{M} = 3 \times 10^{-6} M_{\odot} \text{ yr}^{-1}$

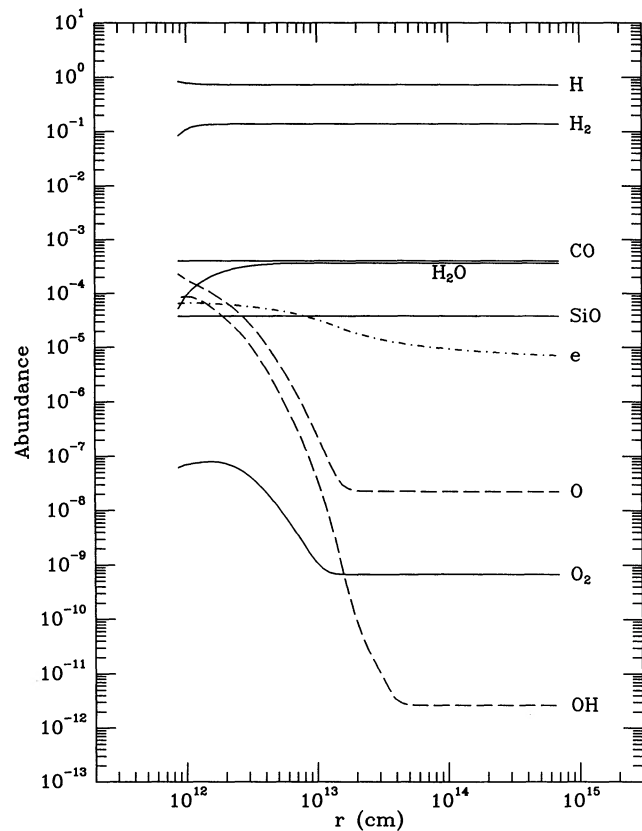


FIG. 5.—Chemical abundances for Case 2 and  $\dot{M} = 3 \times 10^{-5} M_{\odot} \text{ yr}^{-1}$

### 3.3. Case 3: Collimated, Accelerated Wind

This case is closest to the theoretical models of very young, low-mass protostars developed by Shu et al. (1988). Relative to Case 2, the density at the photosphere is another factor of  $V/a$  larger due to the area factor in equation (2). Thus the trend toward efficient neutral molecular synthesis is further enhanced. Another implication of the higher density is that the formation and destruction of molecular hydrogen can now have perceptible thermal effects. Collisional destruction of  $H_2$  cools the gas whereas three-body formation heats the gas because the newly formed (vibrationally excited) molecules are collisionally de-excited at high density. The results of the thermal calculations of RGS in Figure 1 for the intermediate mass-loss rate,  $\dot{M} = 3 \times 10^{-6} M_{\odot} \text{ yr}^{-1}$ , illustrate these effects. RGS also found that ambipolar heating may reheat the gas sufficiently for the  $H_2$  balance to favor collisional dissociation. The reheating depends on the density and the ionization, the latter because ambipolar heating is inversely proportional to  $x_e$ . For the case illustrated in Figure 1, the residual ionization is due to unrecombined  $Na^+$ , i.e.,  $x_e \approx 10^{-6}$ , because  $H^+$  recombines close to the protostar. RGS found even greater reheating for  $\dot{M} = 3 \times 10^{-7} M_{\odot} \text{ yr}^{-1}$  (to  $\approx 4500$  K) but, for  $\dot{M} = 3 \times 10^{-5} M_{\odot} \text{ yr}^{-1}$ , ambipolar diffusion heating merely reduces the rate of decrease in the temperature.

A further consequence of the extremely high initial wind densities in this case is that our integration method becomes difficult to use for mass-loss rates greater than  $\dot{M} = 3 \times 10^{-6} M_{\odot} \text{ yr}^{-1}$ , corresponding to initial densities greater than  $10^{14} \text{ cm}^{-3}$ . As described in § 2, in addition to integrating several hundred chemical rate equations, many with highly disparate time scales, we also implement multiband radiation transfer for each photo-process. The deterioration in our numerical integration capability is manifested by an increased sensitivity to the initial conditions. In order to carry out the calculations for  $\dot{M} = 3 \times 10^{-6} M_{\odot} \text{ yr}^{-1}$ , we start the integrations at somewhat larger radial distances than in the previous cases. Starting at  $1.0 \times 10^{12} \text{ cm}$ , instead of  $6.9 \times 10^{11} \text{ cm}$ , for example, means that the initial density is reduced by a factor of 2.5. This has little effect on the final results because the density is still so high that steady state conditions apply at the start of the integration. We have checked our results by redoing the calculations for a purely neutral chemistry starting at  $R_*$  and find essentially the same asymptotic molecular abundances.

Figure 6 shows our results for  $\dot{M} = 3 \times 10^{-6} M_{\odot} \text{ yr}^{-1}$ . In this case, the temperature (shown in Fig. 1) decreases very rapidly to a minimum of  $\approx 1750$  K at  $2R_*$  and, because of  $H_2$  formation and ambipolar diffusion heating, reaches a maximum of  $\approx 3130$  K at about  $10R_*$ . As found by RGS, the  $H_2$  abundance is reduced from 0.1 to  $\approx 10^{-5}$  by reheating. A similar effect is found for OH and even more so for  $O_2$  and  $H_2O$ , which are closely linked to OH. Unlike  $H_2$ , the abundances of these three oxygen molecules increase again as the temperature drops, but they are more or less frozen beyond  $1000 R_*$ . On the other hand, CO is unaffected by reheating and SiO is reduced by only a factor of 2; the wind beyond  $10R_*$  has roughly equal amounts of SiO and Si.

The results for  $\dot{M} = 3 \times 10^{-7} M_{\odot} \text{ yr}^{-1}$  shown in Figure 7 illustrate the effects of even greater reheating from a temperature minimum of 1350 to 4500 K. In this case, SiO is greatly reduced and even CO has an abundance of only  $5 \times 10^{-7}$ . The high electron fraction in Figure 7 raises the question of whether reheating by ambipolar diffusion really

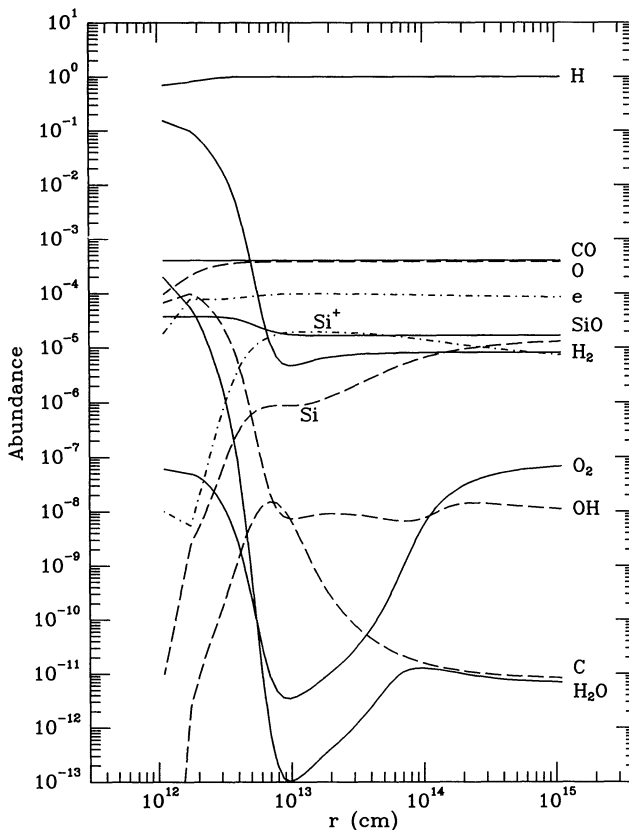


FIG. 6.—Chemical abundances for Case 3 and  $\dot{M} = 3 \times 10^{-6} M_{\odot} \text{ yr}^{-1}$

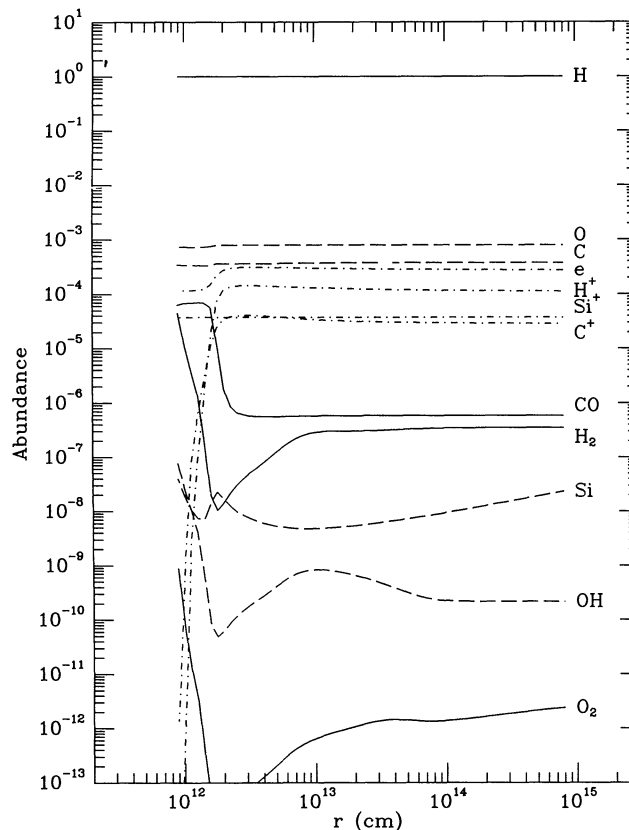


FIG. 7.—Chemical abundances for Case 3 and  $\dot{M} = 3 \times 10^{-7} M_{\odot} \text{ yr}^{-1}$

produces effects as large as those obtained by RGS. In the present calculations, we include the ions of C, S, Si, Mg, Fe, and Al, as well as Na, and find that  $x_e \approx 10^{-4}$ , in contrast to RGS who assumed  $x_e = x_{\text{Na}} = 2.3 \times 10^{-6}$ . Our large electron fraction arises because only  $\text{C}^+$  and  $\text{S}^+$  recombine, although  $\text{Si}^+$  recombines partially for  $\dot{M} = 3 \times 10^{-6} M_\odot \text{ yr}^{-1}$ . Factors of 40 or 50 in  $x_e$  make a big difference in the thermal balance and suggest that the extreme reheating may be an artifact of the low electron fraction assumed by RGS.

In order to further understand the effects of reheating on the chemistry, we calculated the molecular abundances for  $\dot{M} = 3 \times 10^{-7} M_\odot \text{ yr}^{-1}$  without reheating by assuming that the temperature falls monotonically and joins smoothly onto the asymptotic form given by RGS (Appendix C) appropriate to  $x_e = 1.2 \times 10^{-4}$ . The abundances shown in Figure 8 show fewer effects of reheating and 20% of the carbon is in CO.

Finally, the results for the largest mass-loss rate,  $\dot{M} = 3 \times 10^{-5} M_\odot \text{ yr}^{-1}$ , using the RGS temperature distribution are shown in Figure 9. Again we start the integration at  $10^{12}$  cm. In this case, RGS predict little reheating and the wind is essentially molecular. All of the heavy atoms are in the molecules, CO,  $\text{H}_2\text{O}$ , and SiO, etc., and 75% of the protons are in  $\text{H}_2$ . The remaining 25% in atomic hydrogen might, of course, be observable at 21 cm. Most of the atomic ions are recombined; in addition to  $\text{Na}^+$ , 20% of the magnesium remains ionic. Thus the RGS estimate of  $x_e$  is only a factor of 3 too high and the theoretical calculation of the temperature should hold.

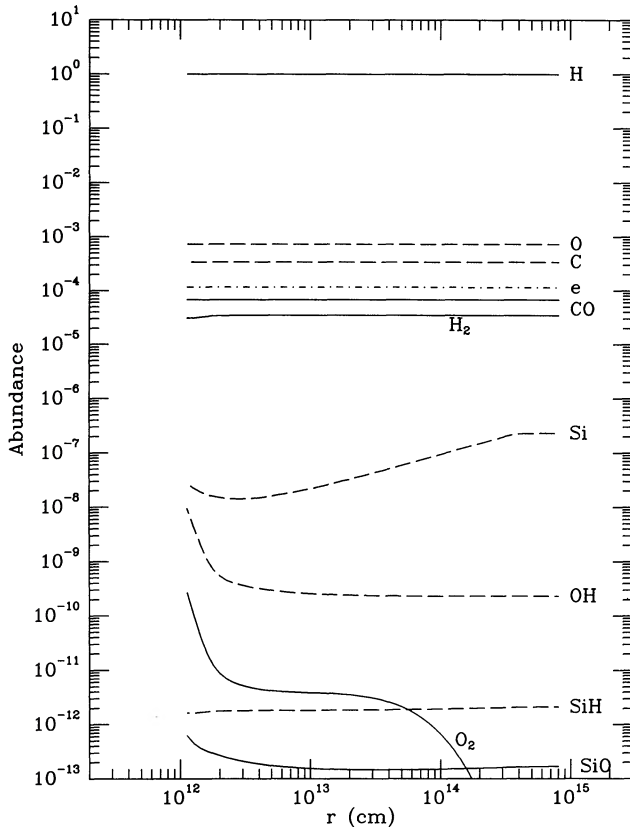


FIG. 8.—Chemical abundances for Case 3 and  $\dot{M} = 3 \times 10^{-7} M_\odot \text{ yr}^{-1}$  for a modified temperature distribution without reheating.

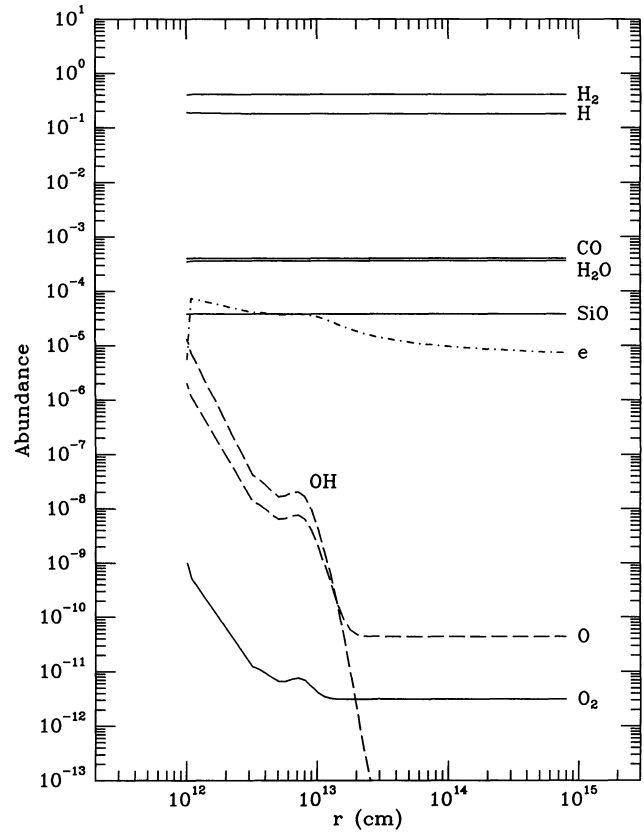


FIG. 9.—Chemical abundances for Case 3 and  $\dot{M} = 3 \times 10^{-5} M_\odot \text{ yr}^{-1}$

#### 3.4. Variations in the Radiation Field

It is obvious that the inner protostellar wind is exposed to a very large radiation field. Its effects can be seen in the occurrence of some very large photorates in Table 3 for a 5000 K blackbody spectrum. Because the density is also large, a proper comparison with other (particle) reaction rates in different astrophysical situations involves the ratio  $G/n$ , where  $G$  is a photorate and  $n$  is the density. In these terms, photo processes that depend on the far-UV band from 900–1100 Å, for example  $\text{H}_2$  and CO photodissociation, are weaker than in the diffuse interstellar medium whereas those that depend on the 1200–2000 Å band, for example  $\text{H}_2\text{O}$  photodissociation and heavy element photoionization, are stronger. In this section, we introduce variations in the protostellar radiation to study how departures from the standard 5000 K blackbody spectrum affect our results.

We first consider changes in the blackbody temperature  $T_*$ . The first three columns of Table 5 offer a comparison between  $T_* = 4000, 5000,$  and  $6000$  K for Case 2 and  $\dot{M} = 3 \times 10^{-6} M_\odot \text{ yr}^{-1}$ . The results for  $T_* = 5000$  K have been discussed in § 3.2 and displayed in Figure 4. We have changed only the photospheric temperature in the new calculations. Although the implied changes in the spectral distribution of the radiation and the total luminosity can, in principle, affect the gas temperature, such effects are actually small (RGS). The results in Table 5 indicate that the basic character of the 4000 and 5000 K winds are similar, i.e., hydrogen is mainly atomic and almost all of the carbon is in CO, but there are differences in SiO and other oxygen-bearing molecules. In particular, oxygen is split equally between O and  $\text{H}_2\text{O}$  for  $T_* = 4000$  K and all of the

TABLE 5  
ASYMPTOTIC ABUNDANCES<sup>a</sup>

X	4000 K	5000 K	6000 K	UV1	UV2
(1)	(2)	(3)	(4)	(5)	(6)
H <sub>2</sub>	6.4–3	1.4–3	4.5–6	6.3–6	4.7–6
e	4.2–5	4.3–5	1.2–4	1.2–4	1.2–4
O	2.9–4	3.5–4	8.0–4	4.5–4	6.0–4
OH	8.9–9	7.0–9	1.2–10	1.7–10	8.4–12
H <sub>2</sub> O	4.1–5	4.7–19	0	0	0
O <sub>2</sub>	1.6–5	3.9–6	5.4–13	7.8–13	1.6–15
C	0	0	4.0–4	5.3–5	2.0–4
C <sup>+</sup>	0	0	2.8–10	5.6–16	3.2–15
CO	4.0–4	4.0–4	1.0–7	3.5–4	2.0–4
CH	0	0	5.4–12	4.2–12	8.6–12
C <sub>2</sub>	0	0	2.7–12	5.0–13	2.8–13
Si	2.6–19	6.2–16	7.5–9	7.5–9	1.8–10
Si <sup>+</sup>	0	0	3.8–4	3.8–4	3.8–4
SiO	3.8–5	3.8–5	3.4–15	4.6–15	9.0–15
S	1.8–5	1.8–5	1.6–5	1.8–5	1.8–5
S <sup>+</sup>	0	0	1.9–6	4.3–15	5.2–15
Fe	3.4–5	3.0–5	5.1–8	5.0–8	1.4–9
Fe <sup>+</sup>	2.0–7	7.5–7	3.4–5	3.4–5	3.4–5
Mg	4.1–6	2.9–8	8.4–8	1.4–7	6.7–9
Mg <sup>+</sup>	3.6–5	3.7–5	4.0–5	4.0–5	4.0–5
Al	6.7–9	6.8–11	1.3–11	9.3–11	5.4–12
Al <sup>+</sup>	3.2–6	3.2–6	3.2–6	3.2–6	3.2–6
Na	5.3–8	3.3–9	1.2–9	6.5–9	9.5–10
Na <sup>+</sup>	2.2–6	2.3–6	2.3–6	2.3–6	2.3–6

<sup>a</sup> Case 2,  $\dot{M} = 3 \times 10^{-6} M_{\odot} \text{yr}^{-1}$ .

silicon remains in SiO; the heavy atoms in this model are also slightly more recombined. By contrast, all molecular abundances are reduced for  $T_{*} = 6000$  K and the ionization is increased by a factor of 3 relative to  $T_{*} = 5000$  K. Even CO is much reduced and, most striking of all, the abundance of SiO is negligible. These substantial changes in going from  $T_{*} = 5000$  to 6000 K are a consequence of the great sensitivity of the abundances of most oxygen-bearing molecules (other than CO) to the far-UV radiation field, which is markedly “harder” at 6000 K.

Next we consider the possibility that the protostellar radiation field is not a pure blackbody, in particular that there may be a significant excess flux in the far-UV. Such an effect might arise in a natural way as the protostar-disk system evolves and the protostar rotation is braked, giving rise to an accretion shock and associated UV emission. We have carried out calculations in which the protostellar spectral energy distribution is blackbody down to a “cutoff” wavelength and constant below that wavelength. There is some observational evidence of T Tauri stars that is suggestive of this type of short-wavelength continuum (Kenyon et al. 1989). The results presented in columns (5) and (6) of Table 5 correspond to cutoff wavelengths of 2000 and 3000 Å, respectively. Although the total excess UV luminosities are small,  $4.0 \times 10^{-3}$  and  $9.8 \times 10^{-2} L_{\odot}$ , respectively, the flux increases at 1000 Å are very large:  $5.5 \times 10^4$  and  $8.8 \times 10^5$  for the cutoffs at 2000 and 3000 Å, respectively. Figure 10 shows the results for the case where the far-UV spectral energy distribution is flat below 2000 Å for Case 2 and  $\dot{M} = 3 \times 10^{-6} M_{\odot} \text{yr}^{-1}$ . Compared with Figure 4 (no UV excess), there are substantial reductions in all molecules but the reduction in the CO abundance is only 15%. The most striking change is that the abundance of SiO is reduced to an extremely low level. Increasing the cutoff wavelength to 3000 Å continues this trend, e.g., the asymptotic CO abundance is reduced by 50%. Although a far-UV excess can be

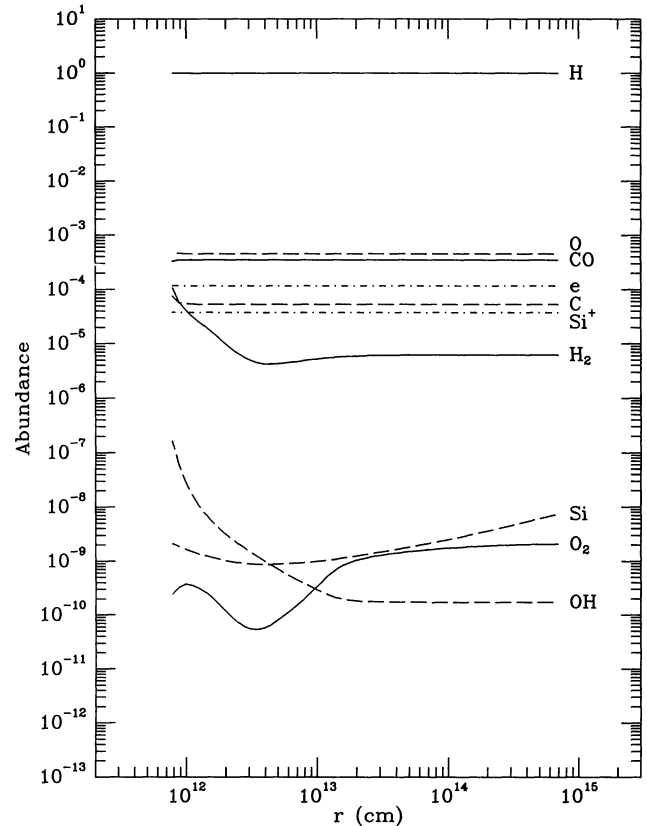


FIG. 10.—Chemical abundances for Case 2 and  $\dot{M} = 3 \times 10^{-6} M_{\odot} \text{yr}^{-1}$  with constant UV energy flux below 2000 Å equal to that of a blackbody at 2000 Å.

very effective in reducing the abundance of many neutral atoms and molecules, the most easily observed molecule CO is fairly resistant to even quite large UV flux increases.

#### 4. DISCUSSION

The results presented in the last section show how molecules can be formed at substantial levels in the very fast, primary winds generated by young, low-mass protostars. The underlying processes proceed efficiently under a wide range of conditions. Even for situations where RGS predicted large reheating, the winds retain a substantial abundance of CO. The most important requirement for molecular synthesis in these winds is that the temperature fall to less than a few thousand K within several protostellar radii. The calculations of RGS are critical in this context because they show how difficult it is to heat the winds in the inescapable presence of cooling associated with adiabatic expansion. We find that the efficiency for molecule formation is greater than in our preliminary report (Paper I), mainly because we now include the density enhancements due to acceleration and collimation. Of course for very low mass-loss rates, such as assumed in the one previous study of the subject by Rawlings et al. (1988), who considered a mass-loss rate,  $\dot{M} = 10^{-9} M_{\odot} \text{yr}^{-1}$ , typical of some T Tauri stars, molecule formation is indeed inefficient.

The calculations also reveal that, given favorable temperatures, molecule formation increases rapidly with the density. Taking into account the effects of expansion, acceleration, collimation, and variations in the mass-loss rate, the calculations span a large range of density. Consequently we have had to implement several types of chemistry, for example

the  $\text{H}^-$ ,  $\text{H}_2^+$ , and  $3\text{H}$  routes to form  $\text{H}_2$  and ion-molecule and neutral reactions to form heavy molecules. The proximity to the protostar also implies that photo effects and the shielding of the protostellar radiation are important. Of particular interest is the crucial role played by charge exchange in the rapid destruction of  $\text{H}^+$  ions and the concomitant increase in the ionization of the wind. The latter effect is due to the fact that the destruction of  $\text{H}^+$  differs from that of the typical heavy atomic ion because it interacts strongly with neutral radicals and molecules. Unfortunately, quantitative results on the ionization of the wind are rendered uncertain by the almost total absence of laboratory measurements of charge exchange reactions in the sub-eV energy range.

The self-shielding of the neutral species subject to photo-destruction also plays a crucial role in molecule formation close to the protostar. Most of the shielding is due to the absorption of photoionizing continuum radiation by the abundant neutral atoms. The effectiveness of an atom in this respect is determined by the photoionization threshold as well as by the abundance of the element and the magnitude of its cross section. Thus, the order in which the ions recombine as the density increases is generally  $\text{C}^+$ ,  $\text{S}^+$ ,  $\text{Si}^+$ ,  $\text{Fe}^+$ ,  $\text{Mg}^+$ ,  $\text{Al}^+$ , and  $\text{Na}^+$ . For CO, which requires photons shortward of  $1100 \text{ \AA}$ , the shielding is produced primarily by C and S atoms. In this context, it is useful to note that, in the least opaque Case 1, equation (2) implies that the optical depth from  $R_*$  to infinity due to C at  $1000 \text{ \AA}$  is more than  $3 \times 10^4$  (for  $\dot{M} = 3 \times 10^{-6} M_\odot \text{ yr}^{-1}$  and  $V = 150 \text{ km s}^{-1}$ ).

Although similar considerations apply to molecular hydrogen, its formation proceeds relatively slowly except at the highest densities. In addition,  $\text{H}_2$  can be readily destroyed by chemical reactions and by collisional dissociation at intermediate temperatures of the order of a few thousand K. It is for these reasons that fast, protostellar winds usually manifest an atomic hydrogen character even where most of the heavy atoms are incorporated in molecules. It is therefore important to keep in mind that the mere detection of atomic hydrogen, e.g., by its 21 cm emission, does not imply the wind is completely atomic. Not only may CO be abundant at relatively low mass-loss rates but, for high mass-loss rates, some hydrogen remains atomic, as shown in Figure 9.

Our calculations are relevant to observations of protostellar winds in the emission lines of various species that can be detected at infrared and radio wavelengths. As we have just mentioned, the short dynamical time scales of protostellar winds ensures that atomic hydrogen is present unless the mass-loss rate is extremely large, i.e., more than  $10^{-4} M_\odot \text{ yr}^{-1}$ . Being quite robust, CO is usually present unless the mass-loss rate is so low that the formation processes are inefficient. The abundance of SiO is more sensitive to density than CO, and the SiO/CO ratio is a tracer of high-density gas. SiO also appears to be particularly sensitive to the presence of excess UV radiation, largely because it has a relatively low threshold energy for photodissociation. However, we know practically nothing about the SiO photodissociation cross section so our ideas on this point are somewhat provisional.

The hydroxyl radical reaches abundances of the order of  $10^{-8}$  and represents a potential diagnostic for intermediate mass-loss rates. Although  $\text{O}_2$  is another indicator of incomplete oxygen chemistry, its abundance is generally small. The abundances of the CH and  $\text{C}_2$  radicals are small and their diagnostic potential for these winds appears to be slight. On the other hand,  $\text{H}_2\text{O}$  is a high-density tracer because it can capture almost all of the residual oxygen not in CO.

There is also considerable interest in the atomic component of these winds. Our calculations show that, except for the largest mass-loss rates, the dominant form of oxygen is atomic. Hence the emission in the fine structure lines in the far-infrared at 63 and  $146 \mu\text{m}$  offers potential diagnostic opportunities. Although carbon is more readily incorporated into CO than oxygen is in  $\text{H}_2\text{O}$ , we find that atomic carbon dominates at low mass-loss rates. In this case, the submillimeter lines at 492 and 809 GHz are of potential interest. In contrast to carbon, silicon occurs in the form of  $\text{Si}^+$  when it is not in SiO, so here the focus is the  $\text{Si}^+$  fine structure line at  $35 \mu\text{m}$ . On the other hand, sulfur will generally be atomic except at the largest mass-loss rates; its fine structure lines are at 25 and  $56 \mu\text{m}$ .

Very high-velocity gas was detected by Lizano et al. (1988) near the highly embedded, protostellar source SSV 13 (with the associated Herbig-Haro objects HH 7 – 11) in both the 21 cm line of atomic H and the 2.6 mm line of CO. They interpreted their observations in terms of a protostellar wind with a mass-loss rate of  $3 \times 10^{-6} M_\odot \text{ yr}^{-1}$  and suggested that this wind drives the extended, lower velocity bipolar outflow, often observed near young stellar objects (e.g., Lada 1985; Snell 1987). Detections of very high-velocity CO with speeds in the range  $100\text{--}200 \text{ km s}^{-1}$  in other sources (Koo 1989, 1990; Margulis & Snell 1989; Giovanardi et al. 1990) lend support to this conclusion. High spatial resolution observations of the HH 7 – 11 outflow (Masson, Mundy, & Keene 1990; Bachiller & Cernicharo 1990) show that it is bipolar with correlated clumps on the two sides of the flow. High-resolution, near-infrared observations of more luminous protostars also provide important evidence for such flows (Mitchell et al. 1989).

At the nominal distance of the HH 7 – 11 source (350 pc), the highest-resolution radio observations ( $12''$ , Bachiller & Cernicharo 1990), probe regions of linear dimension  $6 \times 10^{16} \text{ cm}$  (4000 AU). This is a size scale altogether different from the source of the wind, and it is difficult to comprehend which aspects of the primary wind are being observed with current instrumentation. Our chemical models express some of the qualitative features of the above cited observations. Most important, they explain how the primary wind can be primarily atomic hydrogen for mass-loss rates of the same order as measured in HH 7 – 11 and still contain substantial CO. To make further connections with observations, it will be necessary to understand the excitation of the observed lines and to calculate the line fluxes using radiative transfer techniques that are appropriate for these winds. Eventually, a high-speed primary wind will interact with the surrounding material and undergo significant dynamical and physical changes that include channeling of the flow, entrainment of ambient gas, and shock heating and chemistry. A full understanding of the observations requires consideration of these interactions of the primary wind.

The basic concept of the model investigated in this paper is fairly simple, being based on specified one-dimensional flows and temperature distributions. It is important to keep its limitations in mind as well as the fact that even this "simple" model requires rather elaborate calculations. The assumption of only one spatial dimension is a serious limitation in modeling protostellar evolution involving an accretion disk. We have adopted the RGS method for simulating the effects of collimation on the wind density (Case 3). Similar representations of the changes in the shielding of the protostellar radiation field and inclusion of the radiation emanating from the inner regions of the disk could be implemented. In the longer term,

however, it would be preferable to develop a two-dimensional version of the present calculation.

Our discussion of the ionization and reheating for Case 3 indicates that a more consistent treatment of the thermal effects is needed, one that extends the theory of RGS to include the heavy element chemistry of this paper. It should be recalled that we have emphasized the flow models of RGS in the present calculations and found that the molecular abundances are sensitive to density. The results for other flows may well differ quantitatively, but their qualitative properties should not be much different.

Another assumption of the present calculations, that dust does not form, was made primarily for purposes of simplification but also because it probably has little effect on our general conclusions. As discussed by RGS, dust may form at about  $10 R_*$  but at this point most of the critical molecular synthesis has already occurred. Dust formation can actually help molecular synthesis by shielding wavelength bands longward of  $1200 \text{ \AA}$  that are not shielded by neutral carbon and sulfur. On the other hand, the dust will be silicates and therefore reduce the amount of silicon available for SiO and of oxygen for  $\text{H}_2\text{O}$ .

Another chemical simplification in the present report is the omission of sulfur and nitrogen chemistry. We have actually developed a full sulfur chemistry and are investigating its implications. Because it more than doubles the number of chemical equations, a complete study requires further improvements in our numerical methods in order to deal with the problems mentioned in § 3.3.

We have assumed that the flows are both steady in time and vary smoothly with position. Real winds may be variable and thus clumpy. The strong dependence of the chemistry on density would suggest that the denser parts of a clumpy flow

would be even more molecular, as long as these regions are also well-shielded, and that the more rarefied parts would be more atomic. Even though our present program is one-dimensional, it could be adapted to simulate some aspects of clumpy protostellar winds. Finally, our calculations must eventually break down when the winds begin to interact with ambient interstellar material, particularly with other portions of the nascent cloud. Again some aspects of these interactions could be incorporated into our program but, in principle, they require a two-dimensional theory and the inclusion of shocks.

## 5. CONCLUSION

In conclusion, our calculations reveal the presence of a rich chemistry in the primary winds of young, low-mass protostars. The chemical abundances are sensitive to the basic properties of the flow such as the temperature, the mass-loss rate, and the spatial variation of the density due to the acceleration and collimation of the wind. Our calculations indicate that a variety of atomic and molecular diagnostics of these winds may eventually be able to provide direct information on this important aspect of the formation of stars.

This research has been aided substantially by the NYU Academic Computing Facility. The authors would like to express their appreciation to its staff and director, Max Goldstein, for grants of computing time and other assistance. They would also like to thank V. Escalante and G. Victor for early communication of their results on the carbon atom and A. Dalgarno for helpful discussions of charge exchange and other reactions. This work has been supported by grants from NASA (to A. E. G.) and NSF (to P. J. H.).

## REFERENCES

- Allan, R. J., Clegg, R. E. S., Dickinson, A. S., & Flower, D. R. 1988, *MNRAS*, 235, 1245
- Argyros, J. D. 1974, *J. Phys. B*, 7, 2025
- Bachiller, R., & Cernicharo, J. 1990, *A&A*, in press
- Baulch, D. L., Cox, R. A., Hampson, R. F., Kerr, J. A., Troe, J., & Watson, R. T. 1984, *J. Phys. Chem. Ref. Data*, 13, 1259
- Black, J. H., & Smith, P. L. 1984, *ApJ*, 277, 562
- Brooks, N. H., & Smith, W. H. 1974, *ApJ*, 194, 513
- Chambaud, G., Launay, J. M., Levy, B., Millie, P., Roueff, E., & Tran-Minh, F. 1980, *J. Phys. B*, 13, 4205
- Cohen, N., & Westberg, K. R. 1983, *J. Phys. Chem. Ref. Data*, 12, 351
- Dalgarno, A., Du, M. L., & Yu, J. H. 1990, *ApJ*, in press
- Dalgarno, A., & Lepp, S. 1987, in *Astrochemistry*, ed. M. S. Vardya & S. P. Tarafdar (Dordrecht: Reidel), p. 109
- Escalante, V., & Victor, G. A. 1990, *ApJS*, in press
- Fehsenfeld, F. C., & Ferguson, E. E. 1972, *J. Chem. Phys.*, 56, 3066
- Gear, 1971, *Numerical Initial Value Problems in Ordinary Differential Equations*, (Englewood Cliffs, NJ: Prentice-Hall)
- Giovanardi, F., et al. 1990, private communication.
- Glassgold, A. E., Mamon, G. A., & Huggins, P. J. 1989, *ApJ*, 336, L29 (Paper I)
- Graff, M. M. 1989, *ApJ*, 339, 239
- Graff, M. M., & Dalgarno, A. 1987, *ApJ*, 317
- Graff, M. M., Moseley, J. T., & Roueff, E. 1983, *ApJ*, 269, 796
- Hudson, R. D. 1971, *Rev. Geophys. Space Sci.* 9, 305
- Hudson, R. D., & Kieffer, L. J. 1971, *Atomic Data*, 2, 205
- Karzus, W. J., & Latter, R. 1961, *ApJS*, 6, 167
- Kelly, H. P., & Ron, A. 1971, *Phys. Rev. A*, 5, 168
- Kenyon, S. J., Hartmann, L., Imhoff, C. L., & Cassatella, A. 1989, *ApJ*, 344, 925
- Koo, B.-C. 1989, *ApJ*, 337, 318
- . 1990, *ApJ*, in press
- Lada, C. 1985, *ARA&A*, 23, 267
- Lee, L. C. 1984, *ApJ*, 282, 172
- Leen, T. M., & Graff, M. M. 1988, *ApJ*, 325, 41
- Lepp, S., Dalgarno, A., & McCray, R. M. 1990, *ApJ*, in press
- Lepp, S., & Shull, J. M. 1983, *ApJ*, 270, 578
- Letzelter, C., Eidelsberg, M., Rostas, F., Breton, J., & Thieblemont, B. 1987, *Chem. Phys.* 114, 273
- Lizano, S., Heiles, C. F., Rodriguez, L. F., Koo, B.-C., Shu, F. H., Hayashi, S., & Mirabel, I. F. 1988, *ApJ*, 328, 763
- Mamon, G. A., Glassgold, A. E., & Omont, A. 1977, *ApJ*, 323, 306
- Margulis, M., & Snell, R. L. 1989, *ApJ*, 343, 779
- Masson, C. R., Mundy, L. G., & Keene, J. 1990, *ApJ*, in press
- Mitchell, G. F., Curry, C., Maillard, J.-P., & Allen, M. 1989, *ApJ*, 341, 1020
- Natta, A., Giovanardi, F., Palla, F., & Evans II, N. J. 1988, *ApJ*, 327, 817
- Neufeld, D. A., & Dalgarno, A. 1989a, *ApJ*, 340, 869
- . 1989b, *ApJ*, 344, 251
- Pequignot, D., & Aldrovandi, S. M. V. 1986, *A&A*, 161, 169
- Petuchowski, S. J., Dwek, E., Allen, J. A., & Nuth, J. A. 1989, *ApJ*, 342, 406
- Pouilly, B., Robbe, J. M., Schamps, J., & Roueff, E. 1983, *J. Phys. B*, 16, 437
- Rawlings, J. M. C., Williams, D. A., & Canto, J. 1988, *MNRAS*, 230, 695
- Roberge, W., & Dalgarno, A. 1982, *ApJ*, 255, 176
- Roig, R. A. 1965, *J. Phys. B*, 8, 2939
- Ruden, S. P., Glassgold, A. E., & Shu, F. H. 1990, *ApJ*, 361, 546 (RGS)
- Rutherford, J. A., & Vroom, D. A. 1972, *J. Chem. Phys.*, 57, 3091
- Shu, F. H., Adams, F. C., & Lizano, S. 1987, *ARA&A*, 25, 23
- Shu, F. H., Lizano, S., Ruden, S. P., & Najita, J. 1988, *ApJ*, 328, L19
- Smith, W. H., & Zweibel, E. G. 1976, *ApJ*, 207, 758
- Snell, R. L. 1987, in *Star Forming Regions*, ed. M. Peimbert & M. Jugaku (Dordrecht: Reidel), p. 213
- Stephens, T. L., & Dalgarno, A. 1972, *J. Quant. Spectros. Rad. Transf.*, 12, 569
- Tondello, G. 1972, *ApJ*, 172, 771
- van Dishoeck, E. F. 1987, *J. Chem. Phys.*, 86, 196
- van Dishoeck, E. F., & Dalgarno, A. 1984, *ApJ*, 227, 576
- Wagner, A. F., & Graff, M. M. 1987, *ApJ*, 317, 423
- Wishart, A. W. 1979, *MNRAS*, 187, 50P